Computational Materials Science 134 (2017) 171–183

Contents lists available at ScienceDirect

Computational Materials Science

journal homepage: www.elsevier.com/locate/commatsci

Nonlinear mechanical behaviour of γ-graphyne through an atomistic finite element model

Filipe C. Rodrigues [a], Nuno Silvestre [a,*], Augusto M. Deus [b]

[a] IDMEC, Department of Mechanical Engineering, Instituto Superior Técnico, Universidade de Lisboa, Portugal
[b] CeFEMA, Department of Mechanical Engineering, Instituto Superior Técnico, Universidade de Lisboa, Portugal

ARTICLE INFO

Article history:
Received 13 February 2017
Received in revised form 22 March 2017
Accepted 30 March 2017

Keywords:
γ-Graphyne
Nanomaterials
Finite element model
Mechanical properties
Nonlinear behaviour
Strength

ABSTRACT

A non-linear finite element model for the simulation of the mechanical in-plane behaviour of γ-graphyne is presented in this paper. Different types of bonds (Single C—C, Aromatic C═C, Triple C≡C) are simulated by means of non-linear springs, which accurately take into account the different behaviour of interatomic forces in tension and compression at 0 K temperature. Then, the finite element model is used to conduct six tests (two uniaxial tension–compression tests, one biaxial tension–compression test, two uniaxial shear tests, one biaxial shear test) to evaluate the non-linear mechanical behaviour of γ-graphyne. After that, a set of linear elastic properties (Young's modulus, Poisson's ratio, shear modulus, bulk modulus) and non-linear elastic properties (limit of proportionality stress and strain, ultimate stress and strain) is reported and compared with values reported in the literature (mostly linear elastic properties). This validation shows that the developed finite element model is able to predict accurately the linear and non-linear mechanical properties of γ-graphyne (i.e. stiffness and strength). Additionally, some remarks are drawn regarding the anisotropy of γ-graphyne and its distinct behaviour under tension and compression.

1. Introduction

Carbon has various hybridized states (sp, sp^2 and sp^3), which enable it to bind to itself and with other elements. Diamond and graphite are the most known crystalline forms of this element, but it also has other allotropes, like graphene, carbon nanotubes (CNTs) or the different forms of graphyne [1]. Carbon-based nanomaterials have attracted the interest of researchers in the last few years due to their unique mechanical, electrical, thermal and optical properties [2], allowing the application of these properties in various engineering fields. For example, graphene and CNTs can be used to increase the stiffness and strength of structural composites while decreasing their weight [3] and thermal expansion coefficient [4]. In electronics, CNTs could replace copper on an airplane's wires, turning them lighter and more efficient [5], while graphene and graphyne show promising applications in high-ratio transistors, energy storage and sensors, which could be used to improve electronic systems [6].

γ-Graphyne is a two-dimensional carbon allotrope whose molecular structure is composed of sp and sp^2 hybridized carbon atoms, comprising aromatic hexagonal rings and acetylenic groups as can be seen in Fig. 1. In 2008, Haley [7] presented the synthetic strategies toward, as well as optoelectronic properties of, substructures of the non-natural, graphyne, which is based on the dehydrobenzo 12 annulene framework, but since then there have been no reports of large sheets synthesis [8]. Multiple efforts have been made to develop computational models capable of predicting the mechanical behaviour of γ-graphyne. Cranford and Buehler used Molecular Dynamics (MD) in order to simulate this behaviour, predicting the Young's modulus (533 and 700 [GPa]) and the ultimate stress (48 and 108 [GPa]) for both tested directions [8]. Using Density Functional Theory (DFT) calculations, Peng et al. predicted the in-plane Young's modulus to be 162 [N/m] and the ultimate stress (56 and 59 [GPa]) for both tested directions [9]. Recently, Wang et al. [10] investigated the mechanical properties and fracture behaviours of δ-graphyne and γ-graphyne using MD simulations. They concluded that both graphynes show brittle fracture in uniaxial tension testing at temperatures from 1 to 1200 K

Concerning the out-of-plane behaviour, Becton et al. [11] employed MD simulations to analyze graphynes under geometric confinement across various temperatures, sizes, and crumpling rates and compared them to graphene under the same conditions. They focused on the mechanical stabilizing mechanisms and properties of the crumpled structures. More recently, Lenear et al. [12] also performed MD simulations to examine the folding angle of

* Corresponding author.
E-mail address: nsilvestre@ist.utl.pt (N. Silvestre).

http://dx.doi.org/10.1016/j.commatsci.2017.03.051
0927-0256/

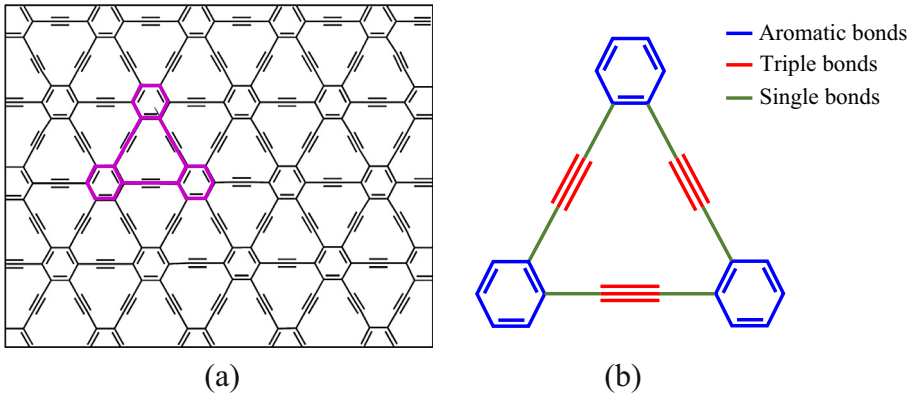

Fig. 1. (a) Scheme of the structure of γ-graphyne [7], (b) detail of the covalent bonds present in γ-graphyne [17].

Table 1
Values of r_0, D_e and β for different bonds.

Bond type	r_0 [nm]	D_e [N m]	β [m^{-1}]
Single (C—C)	0.1407	$6.03 \cdot 10^{-19}$	$2.63 \cdot 10^{10}$
Aromatic (C═C)	0.1426	$1.03 \cdot 10^{-18}$	$4.49 \cdot 10^{10}$
Triple (C≡C)	0.1223	$1.39 \cdot 10^{-18}$	$6.05 \cdot 10^{10}$

graphyne with respect to the linkage number. Also using MD simulations, Wang et al. [13] investigated the out-of-plane behaviour of graphene sheets, namely the evolution of deformation of a monolayer graphene sheet under a central transverse loading. Yang et al. [14] also examined the mechanical properties and failure mechanisms of a graphene sheet containing bi-grain-boundaries. Their results revealed that both temperature and density of defects play key roles in the mechanical behaviour of graphene containing bi-grain-boundaries. Using MD simulations, Yi et al. [15] investigated the mechanical properties of several types of graphynes under pure shearing deformation and bending. They concluded that shear mechanical properties in the zigzag direction are higher than those in the armchair direction and the bending rigidities of graphynes in different directions are almost the same.

The mentioned methods, MD and DFT, require a great amount of computational effort and time investment. In order to overcome this difficulty and based on a molecular mechanics approach, Hou et al. [16] developed an analytical model to obtain closed-form expressions for mechanical properties of graphynes. Also recently, Couto and Silvestre [17] simulated the mechanical behaviour of graphyne using an atomistic finite element method (FEM). The atomistic FEM was used several years ago to assess the mechanical behaviour of carbon nanotubes [18,19], but now it has been extended to other carbon structures. However, to the authors' knowledge, the studies by Hou et al. [16] and Couto and Silvestre [17] were only focused on the graphyne's linear elastic properties. Thus, this work proposes a model based on the atomistic FEM to study the nonlinear mechanical behaviour of γ-graphyne, based on the atomistic equivalent-continuum method first provided by Odegard et al. [20].

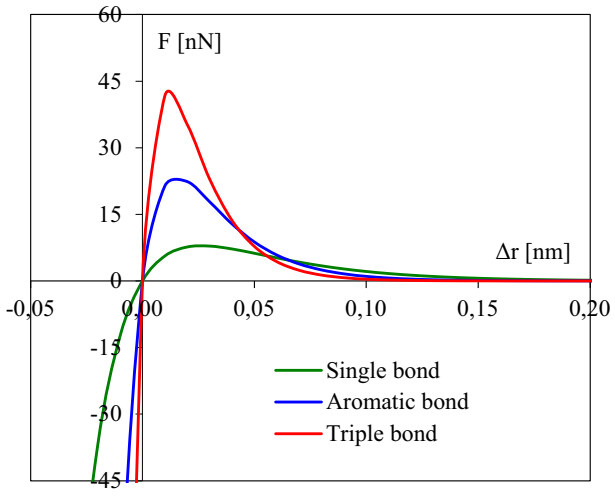

Fig. 2. Force-displacement curves for the simple, aromatic and triple covalent bonds.

2. Non-Linear finite element model

In molecular mechanics, the atomic structure is treated as a system of multiple particles interacting with neighbouring particles. The total interatomic potential energy U_{total} of a nano-structured system is then given by the sum of different energy contributions, as suggested by the following equation:

$$U_{total} = \sum (U_r + U_\theta + U_\phi + U_\omega) + \sum U_{vdw} \tag{1}$$

where the first four terms represent the potential energy of the interactions between bonded atoms, more precisely the stretching U_r and the angle bending U_θ bonds, and the in-plane U_ϕ and out-plane U_ω torsion terms. The last term U_{vdw} corresponds to the potential energy of the van der Waals (vdW) interactions between non-bonded atoms.

All the mentioned interactions can be described by interatomic potentials. The Morse potential [21] has been widely used to describe the U_r and U_θ potentials for single carbon-carbon (C—C) bonds, while the 6–12 Lennard-Jones (L-J) potential [22] is commonly used for the U_{vdw} potential. The next three equations present U_r, U_θ and U_{vdw} above mentioned potentials, respectively.

$$U_r(r) = D_e([1 - e^{-\beta(r-r_0)}]^2 - 1) \tag{2}$$

$$U_\theta(\theta) = \frac{1}{2} k_\theta (\theta - \theta_0)^2 [1 + k_6(\theta - \theta_0)^4] \tag{3}$$

$$U_{vdw}(r) = 4D\left(\frac{d^{12}}{r^{12}} - \frac{d^6}{r^6}\right) \tag{4}$$

The present terms in these equations will be discussed in the next subsections. Using the finite element software ANSYS v.16, the various atomic interactions were modelled using nonlinear (COMBIN39) and linear (COMBIN14) spring elements. In order to

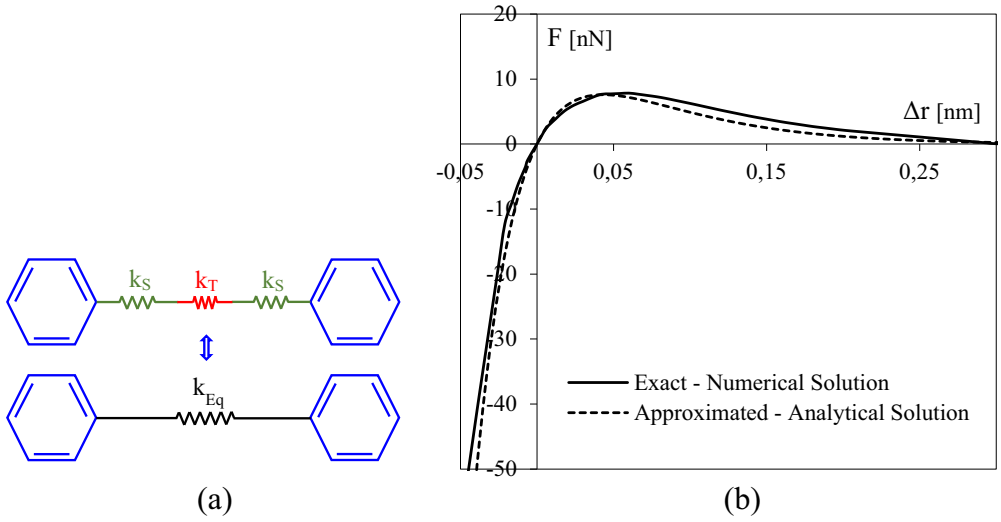

Fig. 3. Stiffness of acetylenic linkage (S-T-S bonds): (a) scheme of the equivalent spring and (b) exact and approximated solutions of F (Δr) curves.

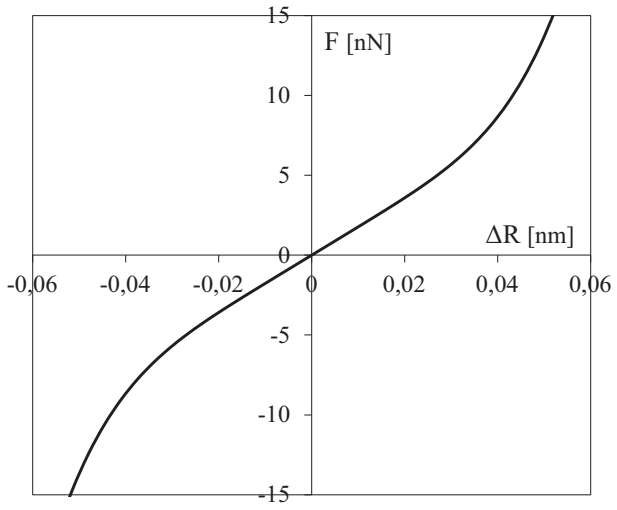

Fig. 4. Variation of force with Δr for spring simulating the angle bending forces.

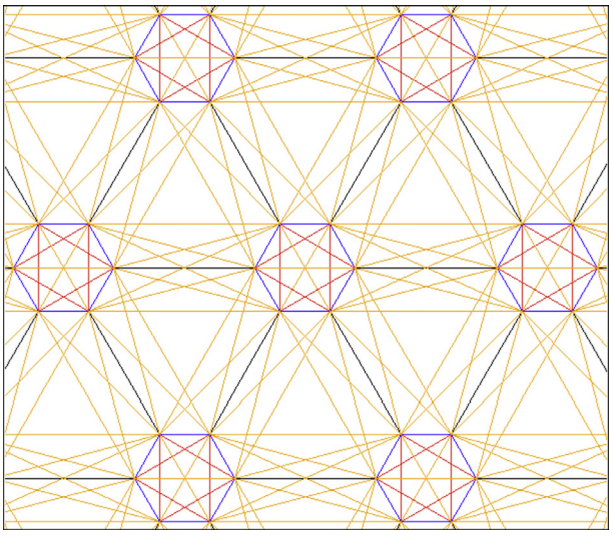

Fig. 5. γ-Graphyne molecule and the aromatic bonds (in blue), S-T-S bonds (in black), springs simulating the vdW forces (in yellow) and springs simulating the angle bending forces (in red). (For interpretation of the references to colour in this figure legend, the reader is referred to the web version of this article.)

apply these potentials, the corresponding force-displacement curves have to be obtained. In the next three subsections, this process will be described.

2.1. Bond axial forces

The structure of γ-graphyne is composed of three types of covalent bonds: single (C—C), aromatic (C═C) and triple (C≡C), as illustrated in Fig. 1(b). To simulate the mechanical behaviour of each bond type, the corresponding force vs. relative displacement F (Δr) curves must be determined. The following expression is obtained from the Morse potential (Eq. (2)):

$$F(\Delta r) = 2D_e\beta(1 - e^{-\beta(\Delta r)})e^{-\beta(\Delta r)} \quad (5)$$

where $\Delta r = r - r_0$ represents the axial deformation of the covalent bond length (relative displacement), D_e corresponds to the dissociation energy (usually denoted as the well depth, defined relatively to the dissociated atoms) and β is a parameter to control the width of the potential well depth. The values from Peng et al. article [9]for the three covalent bonds were used for the initial bond lengths r_0. For the single bond, the values of β and D_e may be found in Belytschko et al. [23]. For the aromatic and the triple bonds, the D_e values were taken from Blanksby and Ellison [24]. These data, valid for temperature of 0 K, is presented in Table 1. Note that the effect of temperature on the mechanical behaviour is relevant, as shown by Wang et al. [10] and Yi et al. [15], but falls outside the scope of this paper. This influence could be achieved by adopting the values of r_0, D_e and β for different temperatures.

Using such data, it was then possible to determine the F(Δr) curves corresponding to the three covalent bond types. These curves are represented in Fig. 2.

In γ-graphyne's structure, the acetylenic linkage consists of a series of single-triple-single (S-T-S) bonds. With the objective of replacing the three individual springs by a single spring in the final model, as illustrated in Fig. 3(a), the equivalent mechanical behaviour of the three bonds was determined. Knowing that the equivalent stiffness of a series of three springs is given by:

$$\frac{1}{k_{Eq}} = \frac{1}{k_S} + \frac{1}{k_T} + \frac{1}{k_S} \quad (6)$$

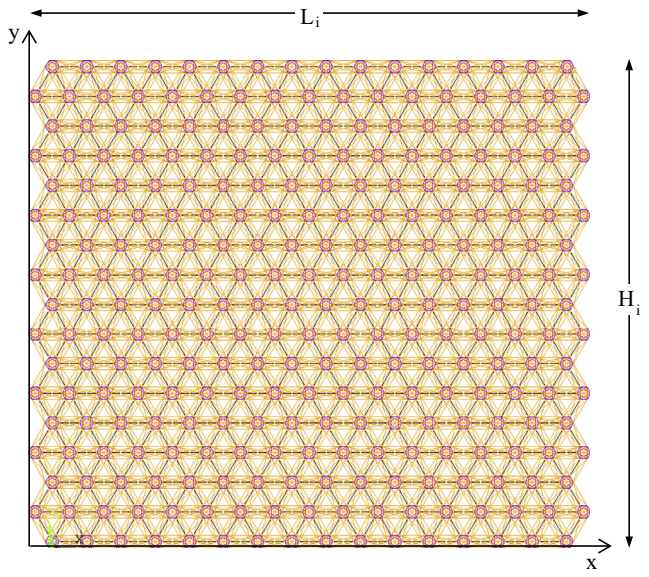

Fig. 6. FE model of γ-graphyne sheet.

The following analytical formula is obtained,

$$k_{Eq} = \left[\frac{2}{\frac{\partial}{\partial(\Delta r)}(2D_e(1-e^{-\beta(\Delta r)})e^{-\beta(\Delta r)})_s} + \frac{1}{\frac{\partial}{\partial(\Delta r)}(2D_e(1-e^{-\beta(\Delta r)})e^{-\beta(\Delta r)})_t} \right]^{-1} \tag{7}$$

After the introduction of Eq. (7) into the general formula,

$$dF = k_{Eq} d(\Delta r) \tag{8}$$

it would then be possible to determine the corresponding F(Δr) curve for the series of S-T-S bonds. However, the integration of Eq. (8) is not straightforward. Instead of using a cumbersome analytical solution, this linkage of three springs was numerically simulated with FEM using nonlinear spring elements. Thus, the force field of this series was calculated and the numerical solution is shown in Fig. 3(b) (solid line). As it turns out, the curve derived from the Morse potential is qualitatively similar to the numerically found curve, so the Morse expression (see Eq. (2) may be adapted to obtain a good fit to the numerical (exact) curve. In this case, the proposed parameter values S-T-S bonds are $D_e = 9.0 \cdot 10^{-19}$ Nm, and $\beta = 1.6 \cdot 10^{10}$ m^{-1}) and the following formula may be used to model acetylenic linkage,

$$F(\Delta r) = 28.8(1 - e^{-16\Delta r})e^{-16\Delta r} \tag{9}$$

with F and Δr given in nN and nm, respectively. The exact (solid line) and approximated (dashed line) F(Δr) curves for the series S-T-S bonds are represented in Fig. 3(b). The maximum tensile force is $F(\Delta r = 0.043 \text{ nm}) = 7.2$ nN.

2.2. Bond bending forces

The angle bending forces were also taken into account on the aromatic benzenic rings. To obtain the respective force field, the derivative form of the corresponding Morse potential for the angle bending bonds (see Eq. (3)) must be determined [25], assuming small angular bond changes $\Delta\theta = (2\Delta R)/r_0$ [20]:

$$F(\Delta R) = \frac{4}{r_0^2} k_\theta (R - R_0) \left[1 + \frac{48}{r_0^2} k_6 (R - R_0)^4 \right] \tag{10}$$

where $R_0 = 0.247[nm]$ is the initial angle bending element length and r_0 is the initial aromatic covalent bond length. The values used for the parameters k_θ and k_6 are $0.9\left[\frac{nN \cdot nm}{rad^2}\right]$ and $0.754[rad^{-4}]$ [23], respectively. The $F(\Delta R)$ curve obtained from the Eq. (9) is presented in Fig. 4. Moreover, the angle bending springs on benzenic aromatic rings are presented in red colour in Fig. 5.

2.3. Non-bonded forces

The interactions of non-bonded carbon atoms can be described by the vdW forces. The derivative form of the 6–12 Lennard-Jones potential, Eq. (4), gives the vdW force field, as shown in the next expression:

$$F_{vdw}(r) = \frac{24 D_{ij}}{d} \left[2\left(\frac{d_{ij}}{r}\right)^{13} - \left(\frac{d_{ij}}{r}\right)^{7} \right] \tag{11}$$

where r is the actual distance between the two non-bonded atoms, D_{ij} corresponds to the bond energy and d_{ij} is a constant that corresponds to the equilibrium atomic distance. For two carbon atoms i and j, D_{ij} and d_{ij} take the values of $4.862 \cdot 10^{-4}$[nN nm] and 0.355 [nm] [26], respectively.

Due to the fact that these interactions are significantly weaker [27] than the stretching or the angle bending ones, it was decided to simplify the model and use them as linear springs. From Eq. (11), it was possible to calculate the vdW spring constant k_{vdw}, as shown below.

$$k_{vdw} = \frac{\partial F_{vdw}}{\partial r} = 1.76 \text{ [nN nm}^{-1}\text{]} \tag{12}$$

Unlike in MD simulations, no cutoff radius was adopted for vdW forces in FE simulations. As shown in Fig. 5, each atom of an aromatic hexagonal ring is connected by linear springs to the seven nearest non-bonded atoms of the closest hexagons and also to the opposed atom in the same aromatic hexagon. These springs provide additional (artificial) stiffness if the atoms are too much apart but there are also other weak interactions that are not accounted through linear springs. Thus, these effects cancel and there is no need to consider the influence of cutoff radius. The schematic present in Fig. 5 shows a detailed molecular segment of γ-graphyne with the respective vdW spring elements represented: the aromatic bonds (in blue), the S-T-S bonds (in black), the springs simulating the vdW forces (in yellow) and the springs simulating the angle bending forces (in red).

2.4. Finite element model and simulations

In order to use the force fields described in the last subsections, the γ-graphyne sheet model was then built. Using the finite element (FE) software ANSYS v.16, a simple γ-graphyne molecule was first modelled using lines. After that, using mirroring commands, it was possible to obtain a complete sheet with the dimensions 10.9 [nm] (L_i) and 9.8 [nm] (H_i) in the armchair (x) and zig-zag (y) directions, respectively. To finish the model the mesh was then made, associating the multiple lines to the respective spring type by applying the force fields described before. The final γ-graphyne sheet nonlinear spring model is presented in Fig. 6.

Using the sheet model presented previously, several analyses can be done to characterize the mechanical behaviour of γ-graphyne. The mechanical properties are calculated using standard elasticity equations [28]. The adopted simulations are:

- Uniaxial tension and compression tests in the armchair (x) direction, with the purpose of acquiring the linear elastic properties (Young's modulus E_x and Poisson's ratio v_{yx}) given by

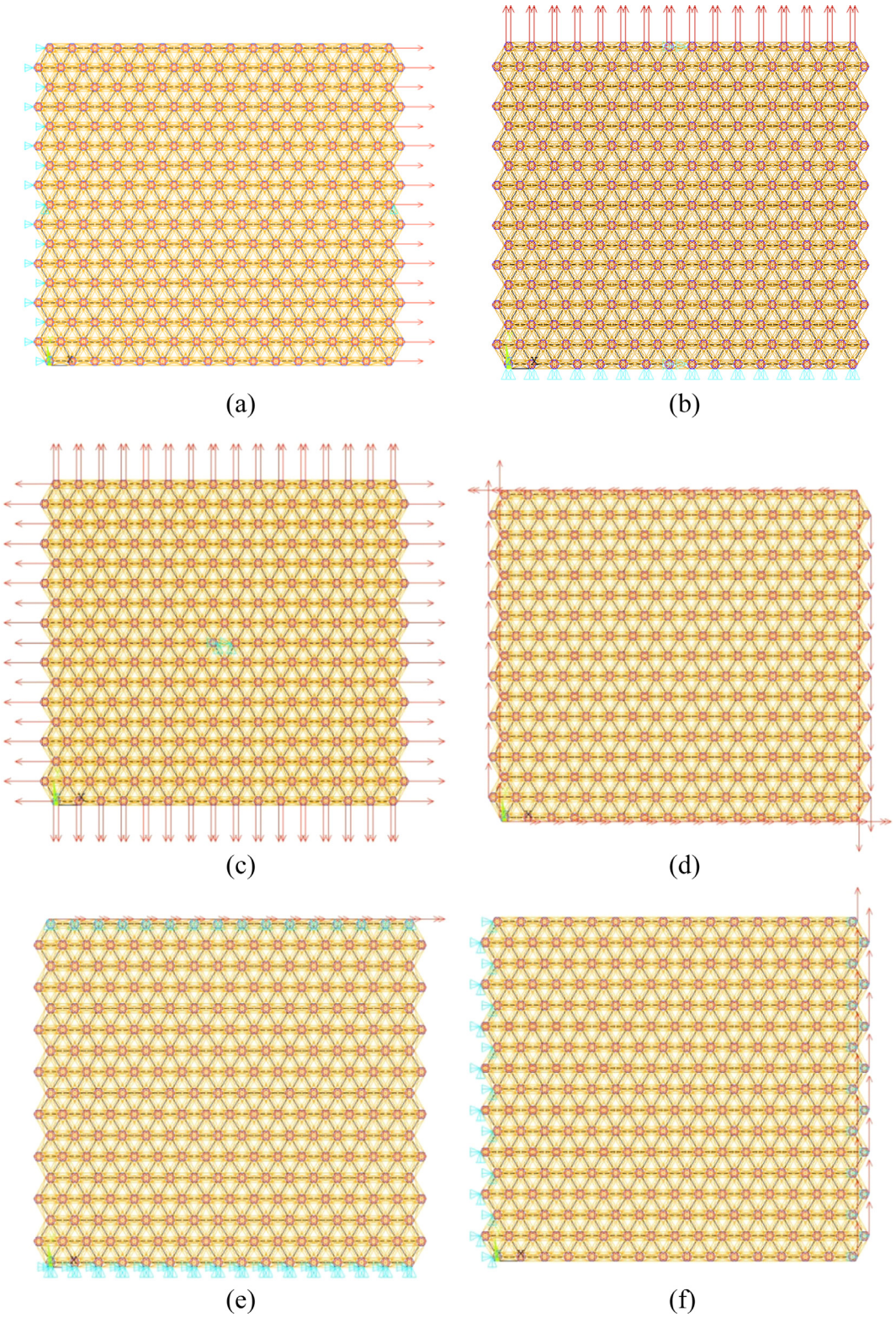

Fig. 7. Boundary and loading conditions of several tests: (a) uniaxial test in (x) direction, (b) uniaxial test in (y) direction, (c) biaxial tension/compression test and (d) biaxial shear test, (e) uniaxial shear test in (x) direction and (f) uniaxial shear test in (y) direction.

$$E_x = \frac{\sigma_x}{\varepsilon_x} \quad \nu_{yx} = -\frac{\varepsilon_y}{\varepsilon_x} \tag{13}$$

where σ_x and ε_x are stress and strain (extension) in the x-axis and ε_y is the strain in y-axis due to Poisson's effect (negative extension). Additionally, the limit of linear elasticity (stress $\sigma_{x,L}$ and strain $\varepsilon_{x,L}$ in x-axis) and the non-linear elastic properties, such as the ultimate stress $\sigma_{x,U}$ and strain $\varepsilon_{x,U}$, are also calculated.

- Uniaxial tension and compression tests in the zig-zag (y) direction, with the purpose of acquiring the linear elastic properties (Young's modulus E_y and Poisson's ratio ν_{xy}) given by

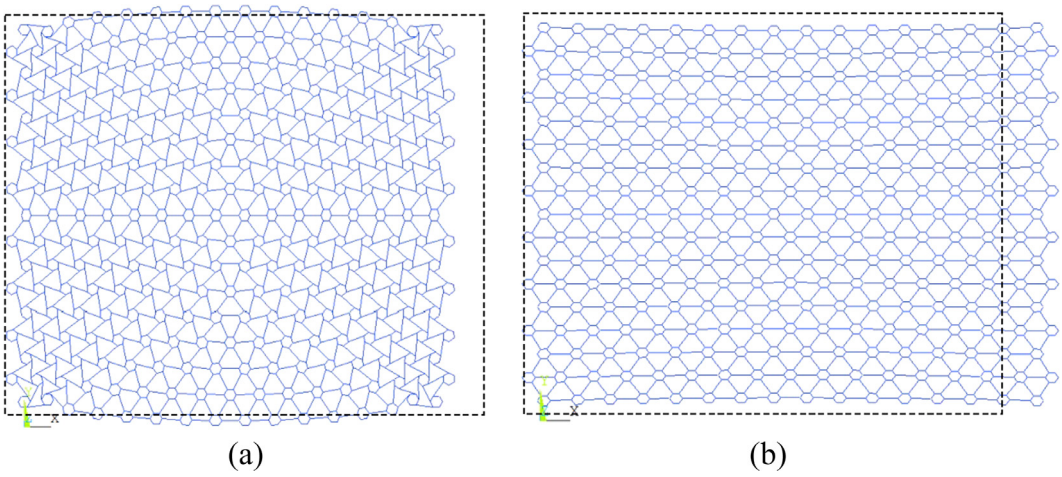

Fig. 8. Sheet deformed shapes in uniaxial test in (x) direction: (a) compression and (b) tension.

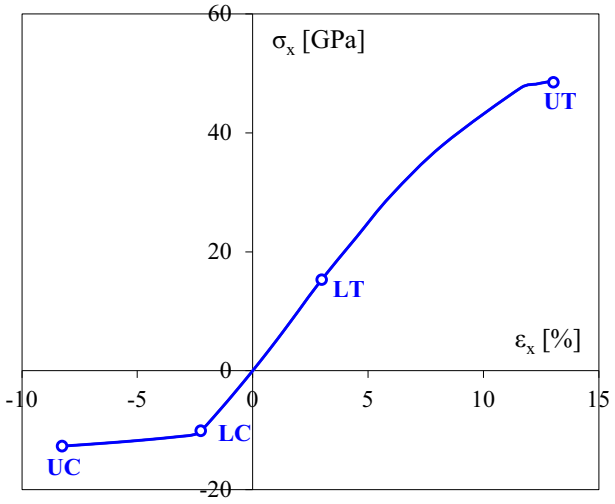

Fig. 9. Stress-strain $\sigma_x(\varepsilon_x)$ curve for the uniaxial analysis in (x) direction and identification of points associated with limit of proportionality ($\sigma_{x,L};\varepsilon_{x,L}$) and ultimate strength ($\sigma_{x,U};\varepsilon_{x,U}$) for both tensile and compressive behaviours.

$$E_y = \frac{\sigma_y}{\varepsilon_y} \quad \nu_{xy} = -\frac{\varepsilon_x}{\varepsilon_y} \tag{14}$$

where σ_y and ε_y are stress and strain (extension) in the y-axis and ε_x is the strain in x-axis due to Poisson's effect (negative extension). The limit of linear elasticity (stress $\sigma_{y,L}$ and strain $\varepsilon_{y,L}$ in y-axis) and the non-linear elastic properties, such as the ultimate stress $\sigma_{y,U}$ and strain $\varepsilon_{y,U}$ are also calculated.

- Biaxial tension and compression tests (xy plane), in order to acquire the linear elastic bulk modulus K_{xy} given by

$$K_{xy} = \frac{\bar{\sigma}}{\varepsilon_A} \quad \bar{\sigma} = \frac{\sigma_x + \sigma_y}{2} \quad \varepsilon_A = \frac{A - A_0}{A_0} \tag{15}$$

where $\bar{\sigma}$ is the average normal stress, ε_A is the surface strain, A_0 is the (initial) area of the undeformed sheet and A is the area of the deformed sheet. Furthermore, the limit of elasticity (average stress $\bar{\sigma}_L$ and surface strain $\varepsilon_{A,L}$ in y-axis) non-linear elastic properties (ultimate average stress $\bar{\sigma}_U$ and corresponding surface strain $\varepsilon_{A,U}$) are also calculated.

- Biaxial shear tests, with the purpose of obtaining the linear elastic shear modulus G_{xy}) given by,

$$G_{xy} = \frac{\tau_{xy}}{\gamma} \tag{16}$$

where τ_{xy} and γ are shear stress and shear strain. The calculation of non-linear elastic properties (ultimate shear stress $\tau_{xy,U}$ and shear strain γ_U) is also intended.

- Uniaxial shear tests in both armchair (x) and zig-zag (y), with the purpose of obtaining the linear elastic shear modulus G_{xy} given by

$$G_{xy} = \frac{G_x + G_y}{2} \quad G_x = \frac{\tau_x}{\gamma_x} \quad G_y = \frac{\tau_y}{\gamma_y} \tag{17}$$

where G_x and G_y are the shear moduli obtained from uniaxial shear tests in x- and y-axis, respectively, τ_x and γ_x are the shear stress and strain obtained in the test for x-axis and τ_y and γ_y are the shear stress and strain obtained in the test for y-axis. The corresponding limit of elasticity and non-linear elastic properties are also calculated.

The imposed boundary and loading conditions for each type of test are depicted in Fig. 7. For all the mentioned analyses, the out-of-plane displacements were fixed (the scope of the paper is the in-plane behaviour of graphyne) and the in-plane displacements were applied in the desired nodes. For each type of analysis, some nodes

Table 2
γ-Graphyne's mechanical properties obtained from the uniaxial tension and compression tests in armchair (x) direction.

Material behaviour	Mechanical property	Tension		Compression	
		[N/m]	[GPa]	[N/m]	[GPa]
Linear elastic	E_x	164.0	512.6	140.8	440.1
	ν_{yx}	0.43		0.42	
Limit of proportionality	$\sigma_{x,L}$	4.9	15.3	3.4	10.6
	$\varepsilon_{x,L}$	0.029		0.024	
Non-linear elastic	$\sigma_{x,U}$	15.6	48.6	4.1	12.7
	$\varepsilon_{x,U}$	0.130		0.083	

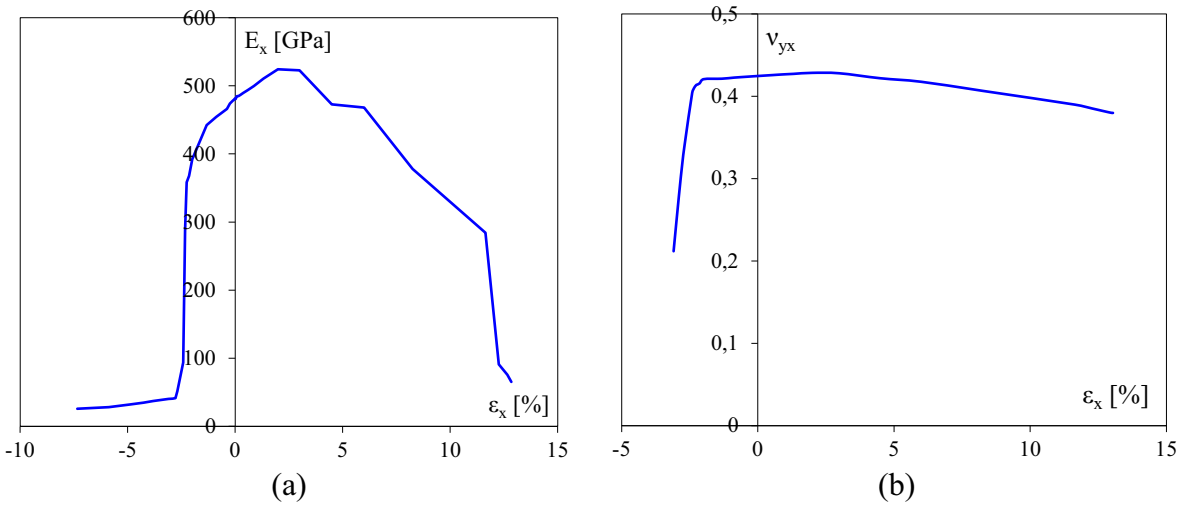

Fig. 10. (a) Variation of tangent elastic modulus with the applied strain for (x) direction, (b) variation of the tangent Poisson's ratio with the applied strain for (x) direction.

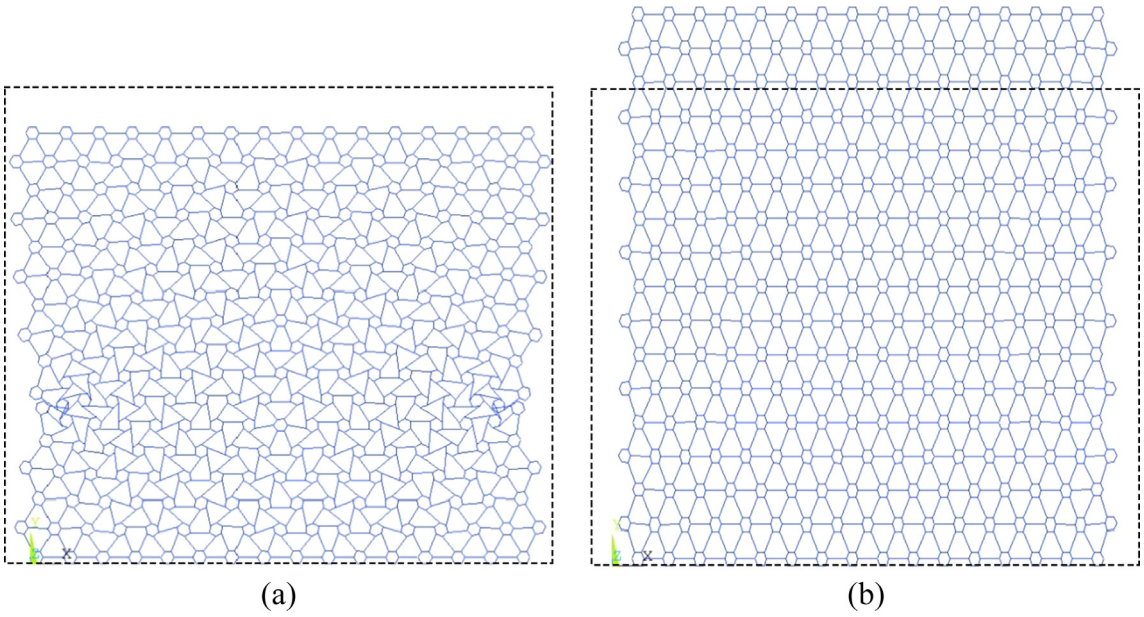

Fig. 11. Sheet deformed shapes in uniaxial test in (y) direction: (a) compression and (b) tension.

were also constrained in order to prevent the rigid body motion and to get the corresponding reaction forces of the nodes. These data are necessary in order to obtain the mechanical properties of γ-graphyne.

3. Results

For the evaluation of the γ-graphyne's mechanical properties, simulations were made using the FE software ANSYS v.16, which uses the Newton-Raphson iterative method to get the converged solutions. The stress-strain curves obtained from incremental-iterative analyses and shown in the next figures correspond to a set of nearly 50–70 equilibrium configurations per test (the number depends on the test). In the next subsections the results obtained will be presented and discussed. In order to give a clearer perception to the reader, the springs that simulate the angle bending and vdW forces are from now on visually omitted. The value of 0.32 nm [8] was adopted as the thickness of the sheet for the obtained results in GPa units.

3.1. Uniaxial tension and compression tests in armchair (x) direction

The applied displacements for these analysis were 1.49 and −0.9 [nm] for the tension and the compression cases, respectively. In Fig. 8, two undeformed and deformed γ-graphyne sheet configurations are presented, corresponding to the last increments of the obtained nonlinear solutions for both tension and compression cases of this analysis. The stress-strain curve, for the uniaxial (x) direction analysis, is presented in Fig. 9. From the curve presented in this plot, for both tension and compression, four points are studied carefully. The limit of linear elasticity points ($\sigma_{x,L}; \varepsilon_{x,L}$) represent the end of proportionality between stresses and strains, while the ultimate strength points ($\sigma_{x,U}; \varepsilon_{x,U}$) correspond to the maximum strength of the sheet in non-linear elastic regime. The limit of elas-

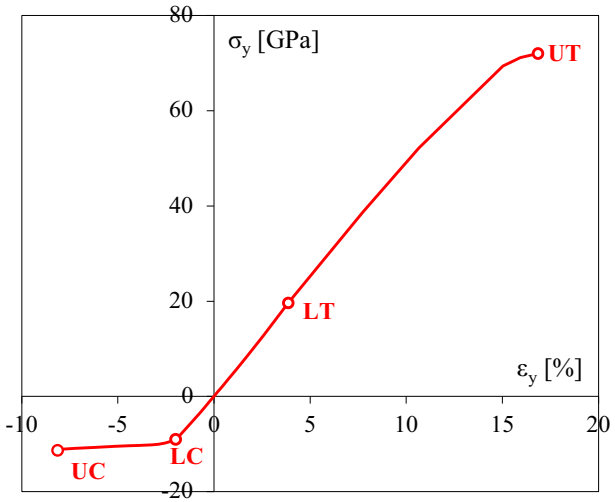

Fig. 12. Stress-strain $\sigma_y(\varepsilon_y)$ curve for the uniaxial analysis in (y) direction and identification of points associated with limit of proportionality ($\sigma_{y,L}; \varepsilon_{y,L}$) and ultimate strength ($\sigma_{y,U}; \varepsilon_{y,U}$) for both tensile and compressive behaviours.

ticity corresponds to the equilibrium configuration at which the tangent modulus (i) ceases its tendency to either remain constant or vary slightly for small strains and (ii) starts to decrease deeply with increasing strains (either tensile or compressive). For the tensile behaviour, this means that the limit of elasticity is achieved whenever the tangent modulus gets negative ($\partial E/\partial \varepsilon < 0$). For the compressive behaviour, the limit of elasticity is achieved whenever the tangent modulus displays a sudden drop for increasing compressive strains (in absolute value). The limit of strength corresponds to the equilibrium configuration at which the tangent modulus changes sign, i.e. turns negative. Despite the stress-strain curve exhibits a very limited descending branch beyond the peak, this is not shown in the following figures. These post-peak paths are very short (meaningless) because the number of iterations to achieve equilibrium is very high and the FE analyses are stopped due to numerical instability (divergence).

Using the data provided by the stress-strain curve, it's possible to calculate the desired mechanical properties of the sheets. The elastic properties, such as the Young's modulus E_x and Poisson's ratio v_{yx}, were evaluated and are shown in Table 2. The variations of these properties with the applied strain ε_x are presented in Fig. 10(a) and (b). Usually, these properties are designated as tangent elastic modulus and tangent Poisson's ratio, and are obtained from the local derivative with respect to ε_x. The values of limit of proportionality stress and strain ($\sigma_{x,L}$ and $\varepsilon_{x,L}$) as well as the ultimate strength values ($\sigma_{x,U}$ and $\varepsilon_{x,U}$), depicted in Fig. 9, are also presented in Table 2. These results will be discussed later.

3.2. Uniaxial tension and compression tests in zig-zag (y) direction

The applied displacements for these analyses were 1.65 and −0.8 [nm] for the tension and the compression cases, respectively. Two undeformed and deformed γ-graphyne sheet configurations are illustrated in Fig. 11, corresponding to the last steps of the obtained nonlinear solutions for both the tension and compression cases of these analyses. The stress-strain curve, for the uniaxial (y) direction analysis, is presented in Fig. 12 and, like for the armchair (x) direction analysis, the limit of elasticity and ultimate points are featured.

From the data provided by the stress-strain curve, it is possible to calculate the desired mechanical properties of the sheets. The Young's modulus E_y and the Poisson ratio v_{xy} were evaluated and are presented in Table 3. The variations of these two properties with the applied strain (tangent elastic modulus and tangent Poisson's ratio) are presented in Fig. 13(a) and (b), respectively. The values of limit of proportionality, stress and strain ($\sigma_{y,L}$ and $\varepsilon_{y,L}$), as well as the ultimate strength values ($\sigma_{y,U}$ and $\varepsilon_{y,U}$), represented in Fig. 12, are also shown in Table 3. These results will be commented later.

3.3. Biaxial tension and compression tests

For the biaxial tests, the applied displacements for these analyses were 0.4 and −0.3 [nm] for the tension and the compression cases, respectively. In Fig. 14, two undeformed and deformed γ-graphyne sheet configurations corresponding to the last step of each case are represented. The variation of average stress $\bar{\sigma}$ with the surface strain ε_A of the sheet is presented in Fig. 15. Using the data provided by the curve $\bar{\sigma}\,(\varepsilon_A)$ of Fig. 15, it is possible to calculate the tangent bulk modulus (obtained from the local derivative of $\bar{\sigma}$ with respect to ε_A). The value of K_{xy} is shown in Table 4 while the variation of tangent bulk modulus with the sheet surface strain ε_A is represented in Fig. 16. The values of limit of elasticity stress and strain ($\bar{\sigma}_L$ and $\varepsilon_{A,L}$) as well as the corresponding ultimate values ($\bar{\sigma}_U$ and $\varepsilon_{A,U}$), represented in Fig. 14, are also shown in Table 4.

3.4. Uniaxial and biaxial shear tests

The applied displacements for the uniaxial and biaxial shear tests were 1.87 and 0.55 [nm], respectively. In Fig. 17, three undeformed and deformed γ-graphyne sheet configurations are presented, corresponding to the last increments of the non-linear solutions for both uniaxial and biaxial shear tests. From the mentioned analyses one can calculate the shear stresses, τ_x and τ_y for the uniaxial tests and τ_{xy} for the biaxial test, and evaluate the corresponding shear strains (γ_x, γ_y and γ_{xy}). The variation of shear stresses with the strains is presented in Fig. 18. From these curves it is possible to calculate the shear modulus G_{xy}. The variation of the tangent shear modulus with the shear strain is also shown in Fig. 19. Additionally, the ultimate stresses and strain for the uniaxial test are shown in Table 5. In case of the biaxial shear test, it was not possible to obtain the ultimate properties due to lack of numerical convergence of the FE-model.

Table 3
γ-Graphyne's mechanical properties obtained from the uniaxial tension and compression tests in armchair (y) direction.

Material behaviour	Mechanical property	Tension		Compression	
		[N/m]	[GPa]	[N/m]	[GPa]
Linear elastic	E_y	162.5	507.8	143.5	451.4
	v_{xy}	0.42		0.40	
Limit of proportionality	$\sigma_{y,L}$	6.3	19.6	2.9	9.0
	$\varepsilon_{y,L}$	0.039		0.019	
Non-linear elastic	$\sigma_{y,U}$	23.0	72.0	3.6	11.2
	$\varepsilon_{y,U}$	0.169		0.082	

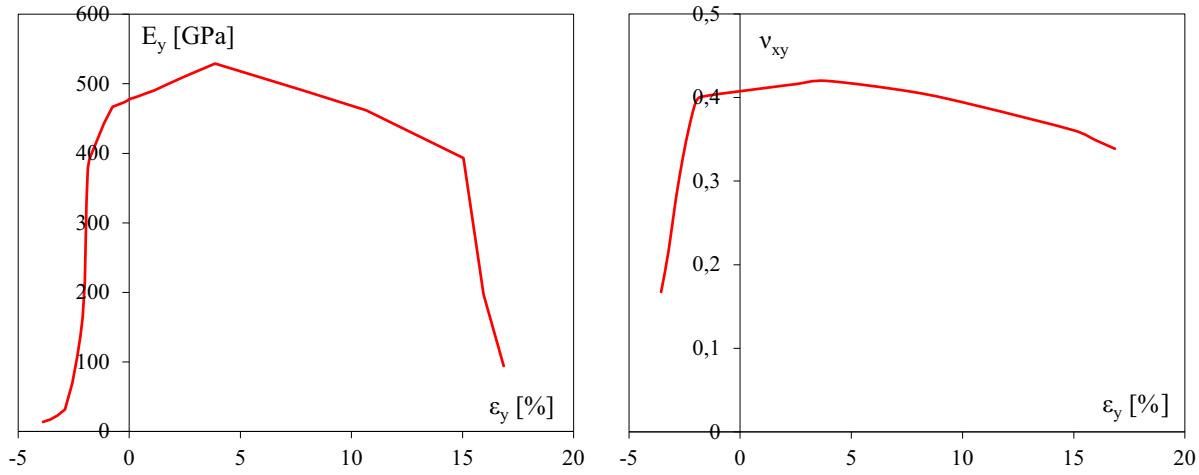

Fig. 13. (a) Variation of tangent elastic modulus with the applied strain for (y) direction; (b) Variation of the tangent Poisson's ratio with the applied strain for (y) direction.

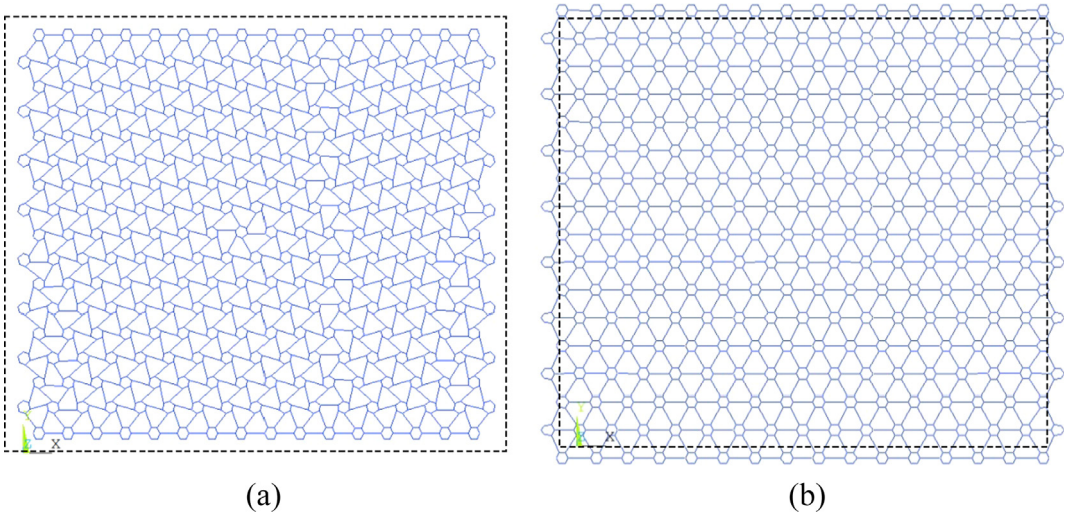

Fig. 14. Sheet deformed shapes in biaxial test: (a) compression and (b) tension.

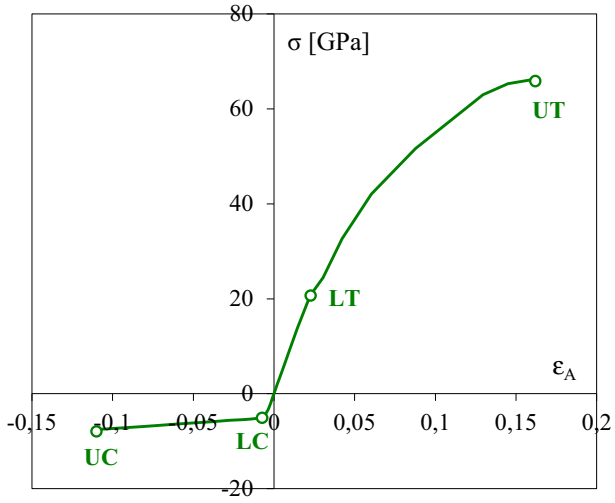

Fig. 15. Stress-strain $\bar{\sigma}(\varepsilon_A)$ curve for the biaxial analysis and identification of points associated with limit of proportionality $(\bar{\sigma}_L; \varepsilon_{A,L})$ and ultimate strength $(\bar{\sigma}_U; \varepsilon_{A,U})$ for both tensile and compressive behaviours.

3.5. Discussion

In this subsection, the results obtained for the linear elastic, limit of linear elasticity and non-linear elastic properties (presented in previous section) will be discussed next. For comparison purpose, some results reported in the literature and obtained from different techniques, such as MD, DFT and FEM, are shown in Tables 6 (linear elastic properties) and Table 7 (limit of elasticity and non-linear elastic properties). In order to distinguish between tensile and compressive properties, the subscripts T and C will be used for tension and compression, respectively.

First, the linear elastic properties will be discussed. From the uniaxial tests, it was predicted that γ-graphyne exhibits a slightly orthotropic behaviour for both tension and compression cases. Moreover, γ-graphyne also shows a clear distinct behaviour under tensile and compressive loadings. The Young's moduli for the tension tests were $E_{x,T} = 512.6$ GPa (x-axis) and $E_{y,T} = 507.8$ GPa (y-axis), with 1% difference. These results are in good agreement with those presented in literature, especially with the ones that were obtained with MD. In case of the x-direction, the differences between the calculated $E_{x,T}$ values and those found in the literature were: 2.4% [32], 3.9% [8], 5.5% [29] and 14.0% [30]. In case of the

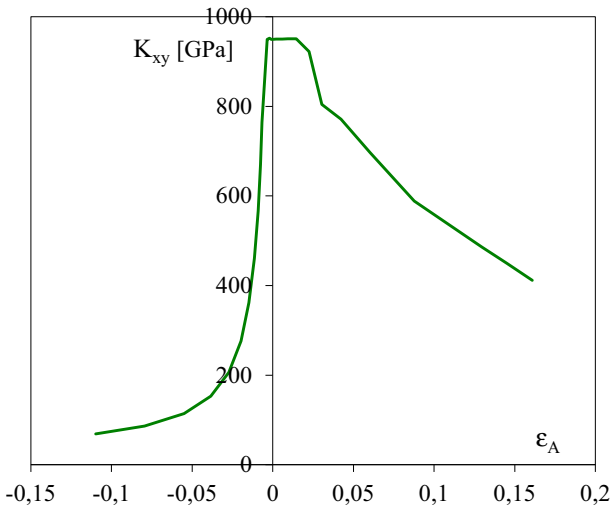

Fig. 16. Variation of tangent bulk modulus with the surface strain for the biaxial analysis.

y-direction, the differences between the calculated $E_{T,y}$ values and those found in the literature were: 0.4% [30] 0.9% [32] and 37.0% [8]. For $E_{x,T}$ and $E_{y,T}$, the differences found between the results of the FE model proposed by Couto and Silvestre [17] and the literature values were higher than in the present study. This is because the model proposed by Couto and Silvestre [17] is based on beam elements, which depend on the cross-sectional parameters (geometry and dimensions), rather than on the bond stiffness itself (like the spring model proposed herein).

Regarding the Poisson's ratio, the values agree with those found in the literature. However it should be mentioned that these are transformed values. The values of Poisson's ratio calculated directly from the FE model (between 0.66 and 0.73) were always higher than the maximum allowable value of 0.5 for three-dimensional stress states. However, in these models, (i) the sheets are purely two-dimensional (there is no thickness dimension) and (ii) uniform displacements were imposed to the γ-graphyne sheets, leading to plane-strain state rather than plane-stress (this would be the case if uniform forces were applied at the edges of γ-graphyne sheets). In case of plane-strain elasticity, the relation between two-dimensional (2D) and three-dimensional (3D) Poisson's ratios was derived by Eischen and Torquato [34] and reads

$$\nu^{3D} = \frac{\nu^{2D}}{1+\nu^{2D}} \tag{18}$$

where ν^{2D} and ν^{3D} are the 2D and 3D Poisson's ratios, respectively. Using this relation, the calculated Poisson's ratios (higher than 0.5) were converted from 2D to 3D. The values of 3D Poisson's ratios, shown in tables 2 and 3 (below 0.5), are in good agreement with the majority of results reported in literature.

For the biaxial tension case, the value of surface bulk modulus $K_{xy} = 295.1$ N/m was obtained. This result shows a small difference (5.1%) with respect to the one obtained by Rouhi et al. [31] using MD. However, it also shows differences of 50% when compared to the DFT results of Asadpour et al. [33] and Peng et al. [9]. For the biaxial shear test, the shear modulus $G_{xy} = 127.11$ [GPa] was calculated, which is in good agreement with the result obtained by Zhao et al. [32], with a 1.2% difference. However, the results obtained by Asadpour et al. [33] and Peng et al. [9] display a difference of 80%. In the case of uniaxial shear tests, the value of G_{xy} was found 24% lower than that of biaxial test. This evidence shows that the uniaxial shear tests cannot be used to evaluate the value of G_{xy}. The reason for this underestimation is that the sheet in uniaxial shear test is not under pure shear but a combination of shear and in-plane bending. For instance, in the uniaxial shear test in x-axis (see Figs. 7(e) and 17(a)), the horizontal shear forces applied at the top edge of sheet and the reaction forces at the bottom edge are in equilibrium of horizontal forces but not in equilibrium of moments. These unbalanced forces and reactions generate not only shear strains but also bending strains that lower unreasonably the value of G_{xy}.

Regarding the limit of proportionality and non-linear elastic properties, some remarks may also be drawn. First, the stress σ_L and strain ε_L were attributed to the limit of proportionality of stress-strain curves (end of proportionality) while the stress σ_U and strain ε_U were also identified, corresponding to the local maxima of the stress-strain curves. By observing Figs. 10(a) and 13(a), it should be noted a slight variation of the tangent elastic moduli in the range between the compressive and tensile strains associated to the limit of proportionality. This is due to the existence of a marginal softening in compression and hardening in tension that influences the stiffness of the sheet and implies slightly non-uniform tangent elastic moduli in linear elastic regime. Note also that this effect vanishes in the biaxial tension and compression tests as the tangential bulk modulus remains uniform (~ 922 GPa) in the linear elastic range ($-0.006 < \varepsilon_A < 0.022$), as depicted in Fig. 19. Additionally, by looking at the stress-strain curves shown in previous section, it can be concluded that the stiffness (tangent elastic modulus) of the sheet starts decreasing after the limit of proportionality point, for both tension and compression cases (see Figs. 10(a) and 13(a)), as well as the Poisson's ratio (see Figs. 10(b) and 13(b)). Like in the linear elastic regime, it is noted a different behaviour between the tension and compression cases for non-linear regime. For all the analyses, regardless of being uniaxial or biaxial, the stresses corresponding to the limit of proportionality and ultimate strength are always lower in compression than in tension. The same occurs for the strains.

The ultimate values for the tension tests were $\sigma_{x,TU} = 48.6$ [GPa] and $\varepsilon_{x,TU} = 13.0\%$, and $\sigma_{y,TU} = 72.0$ [GPa] and $\varepsilon_{y,TU} = 16.9\%$, for the (x) and (y) directions, respectively. The bigger values verified for the (y) direction may be explained considering that there is a greater number of acetylenic groups aligned with the direction of the imposed displacements [8]. These results, showing an orthotropic behaviour for the sheets' strength properties, are in good agreement with the majority of those found in the literature. For direction (x), the lowest verified differences between the calculated

Table 4
γ-Graphyne's mechanical properties obtained from the biaxial tension and compression tests.

Material behaviour	Mechanical property	Tension		Compression	
		[N/m]	[GPa]	[N/m]	[GPa]
Linear elastic	K_{xy}	295.1	922.2	303.8	949.3
Limit of proportionality	$\bar{\sigma}_L$	6.6	20.7	1.6	5.1
	$\varepsilon_{A,L}$	0.022		0.006	
Non-linear elastic	$\bar{\sigma}_U$	21.2	66.2	2.4	7.6
	$\varepsilon_{A,L}$	0.16		0.11	

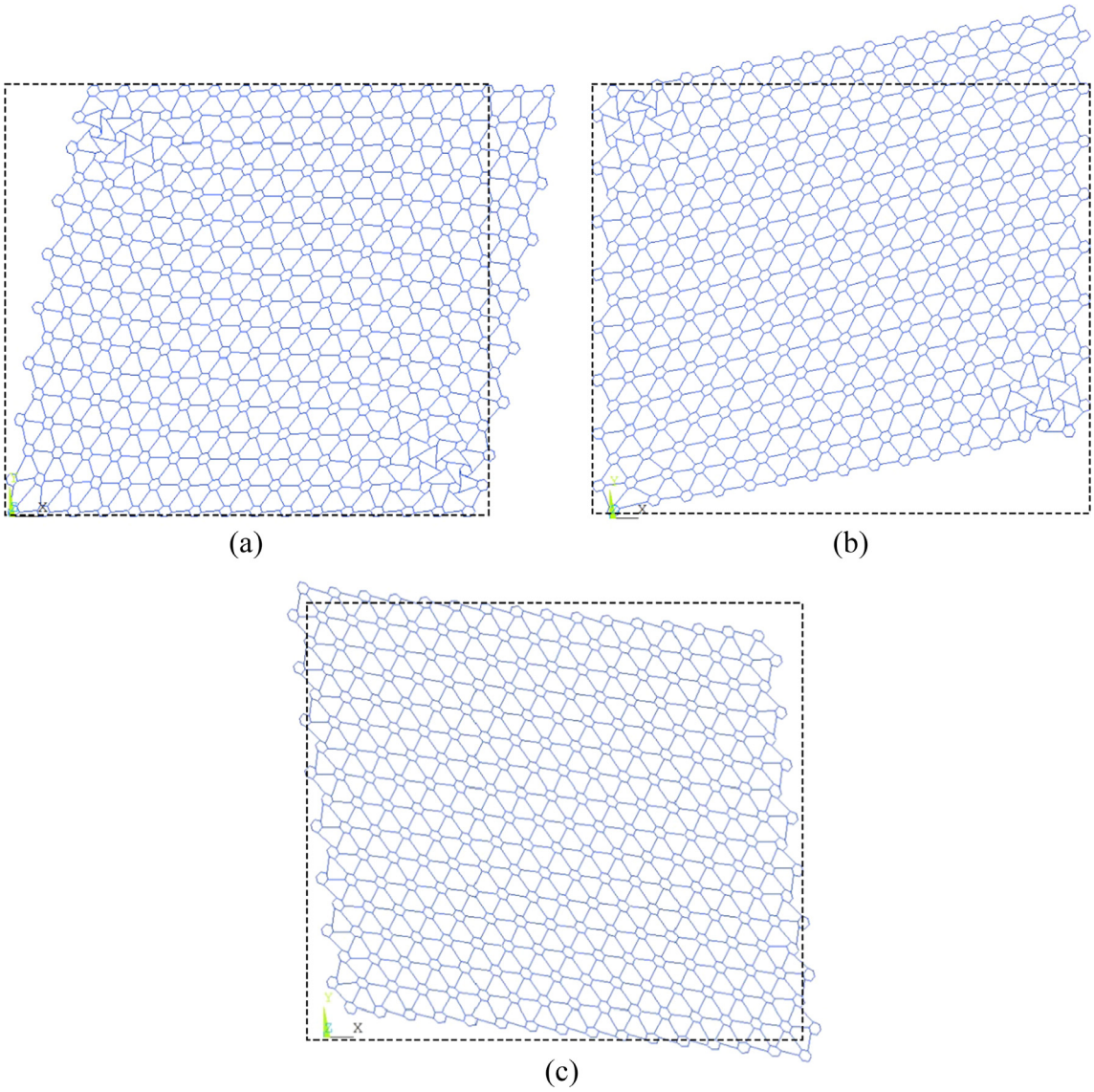

Fig. 17. Sheet deformed shapes in shear tests: (a) Uniaxial test in (x) direction, (b) Uniaxial test in (y) direction, (c) Biaxial test.

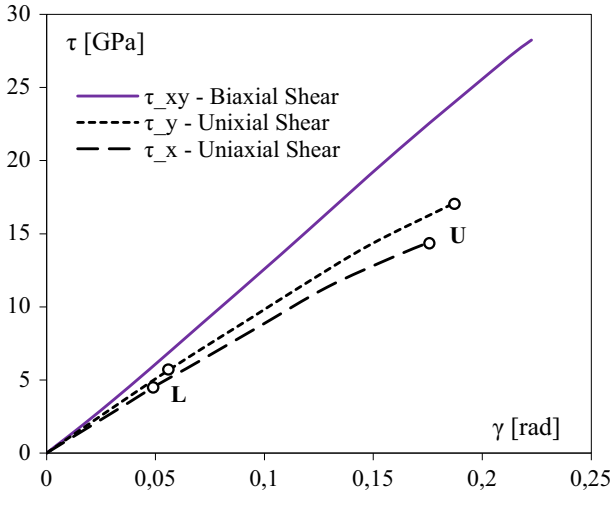

Fig. 18. Shear stress-strain $\tau(\gamma)$ curve for both uniaxial and biaxial analyses and identification of points associated with limit of proportionality $(\tau_L; \gamma_L)$ and ultimate strength $(\tau_U; \gamma_U)$ for the uniaxial analyses.

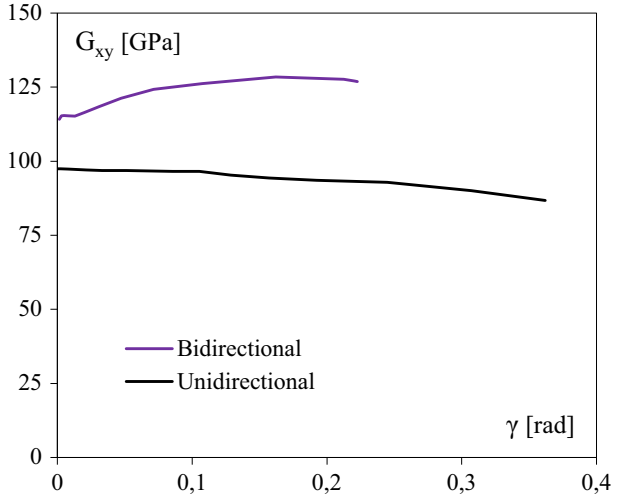

Fig. 19. Variation of tangent shear modulus with the shear strain for both uniaxial and biaxial analyses.

Table 5
γ-Graphyne's mechanical properties obtained from the uniaxial and biaxial shear tests.

Behaviour	Mechanical property	Uniaxial		Biaxial	
		[N/m]	[GPa]	[N/m]	[N/m]
Linear elastic	G_{xy}	30.9	96.6	40.7	127.1
Limit of proportionality	$\tau_{x,L}$	1.5	4.6	n.a.	
	$\gamma_{x,L}$	0.051			
	$\tau_{y,L}$	1.8	5.5		
	$\gamma_{y,L}$	0.055			
Non-linear elastic	$\tau_{x,U}$	4.6	14.4		
	$\gamma_{x,U}$	0.18			
	$\tau_{y,U}$	5.5	17.1		
	$\gamma_{y,U}$	0.19			

Table 6
Comparison of γ-Graphyne's linear elastic mechanical properties obtained from the present work and others available in literature.

Method (authors)	E_x N/m (GPa)	ν_{yx}	E_y N/m (GPa)	ν_{xy}	K_{xy} N/m (GPa)	G_{xy} N/m (GPa)
FEM (present work)	164.0 (512.6)	0.43	162.5 (507.8)	0.42	295.1 (922.2)	40.7 (127.1)
MD [8]	170.4 (532.5)	–	224.0 (700.0)	–	–	
MD [29]	155.0	–	150.0	–	–	
MD [30]	(586.0)	0.48	(510.0)	0.64	–	
MD [31]	140.0	–	130.0	–	280.0	
MD [32]	(525.0)	0.17	(503.1)	0.19	–	(128.6)
DFT [33]	–	–	–	–	122.7	77.0
FEM [17]	229.9 (718.5)	0.42	209.8 (655.7)	0.40	166.0	71.0

Table 7
Comparison of γ-Graphyne's non-linear elastic mechanical properties obtained from the present work and others available in literature.

Method (authors)	$\sigma_{x,U}$ N/m (GPa)	$\varepsilon_{x,U}$	$\sigma_{y,U}$ N/m (GPa)	$\varepsilon_{y,U}$	$\bar{\sigma}_U$ N/m (GPa)
FEM (present work)	15.6 (48.6)	0.13	23.0 (72.0)	0.17	6.6 (20.7)
MD [8]	(48.2)	0.08	(107.5)	0.13	–
MD [29]	14.4	0.11	20.47	0.12	–
MD [30]	(55.6)	0.12	(53.7)	0.14	–
MD [32]	23.8	0.18	30.8	0.25	–
DFT [9]	–	–	–	–	20.6

and reported values for the $\sigma_{x,TU}$ were 0.8% [29] and 7.7% [8], while for direction (y) the lowest differences were 11% [29] and 18.3% [9]. For both directions, the differences for the ultimate strain values varied between 10% and 18%, while the highest differences for ultimate stress and strain values were roughly 40% [8]. In the non-linear elastic regime, the Poisson's ratio decreased with the increase of imposed strain. For the biaxial tension test, the ultimate mean stress was $\bar{\sigma}_U = 6.6$ [N/m] and the ultimate surface strain was $\varepsilon_{A,U} = 2.24\%$. It was noted that K_{xy} decreases as well in non-linear elastic regime (see Fig. 19). For the biaxial shear test, the obtained results demonstrated a linear relationship between the shear stress and shear strain up to the maximum stress, so it can be concluded that the sheet didn't reach the non-linear regime. A qualitatively different result was found for the uniaxial shear tests, in which the shear stress varied non-linearly with the shear strain (see Fig. 18). For increasing values of shear strain, it was noted a small (marginal) increase of the tangent shear modulus obtained from the biaxial shear test while a small decrease was observed for the uniaxial shear tests (see Fig. 19).

4. Conclusion

The non-linear mechanical in-plane behaviour of perfect γ-graphyne was simulated and characterized by means of an atomistic finite element model. To the authors' knowledge, this is the first time such a non-linear finite element model is proposed to study γ-graphyne. The model was explained and the different types of bonds (Single C—C, Aromatic C═C, Triple C≡C) were simulated by means of non-linear springs, which accurately take into account the different behaviour of interatomic forces in tension and compression. Then, the finite element model is used to conduct six tests (two uniaxial tension-compression tests, one biaxial tension-compression test, two uniaxial shear tests, one biaxial shear test) to evaluate the non-linear mechanical behaviour of γ-graphyne. After that, a set of linear elastic properties (Young's modulus, Poisson's ratio, shear modulus, bulk modulus) and non-linear elastic properties (yield stress and strain, ultimate stress and strain) is reported and compared with values reported in the literature (mostly linear elastic properties). The following conclusions may be drawn from the present study:

- The non-linear force-displacement curve for the acetylenic linkage was fairly well approximated by a series of single-triple-single (S-T-S) bonds. To the authors' knowledge, original parameter values ($D_e = 9.0 \cdot 10^{-19}$ Nm and $\beta = 1.6 \cdot 10^{10}$ m^{-1}) were originally proposed herein to simulate acetylenic links through Eq. (9).

- The finite element model developed for the perfect γ-graphyne sheet provided good predictions of both linear and non-linear elastic properties of γ-graphyne, compared to MD and DFT results.
- The γ-graphyne exhibited orthotropic behaviour regarding both stiffness (linear elastic properties) and strength (non-linear elastic properties). This orthotropy has also been reported by other researchers.
- The γ-graphyne exhibited a markedly distinct behaviour under tension and under compression. Despite the fact that out-of-plane displacements are omitted, γ-graphyne is still much stiffer and stronger under tension than under compression, as expected.
- The proposed finite element model may be easily extended for other types of graphynes, such as α-graphyne, β-graphyne, δ-graphyne and 6,6,12-graphyne.

Acknowledgements

This work was supported by FCT, through IDMEC, under LAETA, project UID/EMS/50022/2013.

References

[1] M.I. Katsnelson, Graphene: carbon in two dimensions, Mater. Today 10 (2007) 20–27.
[2] C. Cha, S. Shin, N. Annabi, M. Dokmeci, A. Khademhosseini, Carbon-based nanomaterials: multifunctional materials for biomedical engineering, ACS Nano 7 (2013) 2891–2897.
[3] S. Bellucci, C. Balasubramanian, F. Micciulla, G. Rinaldi, CNT composites for aerospace applications, J. Exp. Nanosci. 2 (2007) 193–206.
[4] S.H. Pezzin, L.A.F. Coelho, S.C. Amico, New generation of multifunctional composites with carbon nanotubes for space applications, Polymers in Defence & Aerospace Applications 2010 Conference, Proceedings, Hamburg, Germany, 2010, pp. 1–28.
[5] T. Kukowski, Lightweight CNT cables for aerospace, in: ESC NDE Technology Assessment NASA NDI Workshop, Johnson Space Center, Houston, TX, 2012.
[6] Q. Peng, A.K. Dearden, J. Crean, C. Liang, H. Sheng, S. De, New materials graphyne, graphdiyne, graphone, and graphane: review of properties, synthesis, and application in nanotechnology, Nanotechnol. Sci. Appl. 7 (2014) 1–29.
[7] M.M. Haley, Synthesis and properties of annulenic subunits of graphyne and graphdiyne nanoarchitectures, Pure Appl. Chem. 80 (2008) 519–532.
[8] S.W. Cranford, M.J. Buehler, Mechanical properties of graphyne, Carbon 49 (2011) 4111–4121.
[9] Q. Peng, W. Ji, S. De, Mechanical properties of graphyne monolayers: a first-principles study, Phys. Chem. Chem. Phys. 14 (2012) 13385–13391.
[10] S. Wang, Z. Fan, Y. Cui, S. Zhang, B. Yang, H. Chen, Fracture behaviors of brittle and ductile 2D carbon structures under uniaxial tensile stress, Carbon 111 (2017) 486–492.
[11] M. Becton, L. Zhang, X.Q. Wang, Mechanics of graphyne crumpling, Phys. Chem. Chem. Phys. 16 (34) (2014) 18233–18240.
[12] C. Lenear, M. Becton, X.Q. Wang, Computational analysis of hydrogenated graphyne folding, Chem. Phys. Lett. 646 (2016) 110–118.
[13] S. Wang, B. Yang, S. Zhang, J. Yuan, Y. Si, H. Chen, Mechanical properties and failure mechanisms of graphene under a central load, ChemPhysChem 15 (2014) 2749–2755.
[14] B. Yang, S. Wang, Y. Guo, J. Yuan, Y. Si, S. Zhang, H. Chen, Strength and failure behavior of a graphene sheet containing bi-grain-boundaries, RSC Adv. 4 (2014) 54677–54683.
[15] L. Yi, Y.Y. Zhang, X. Q Feng, T.C. Chang, J. Wang, J.K. Du, J. X Zhou, Mechanical properties of graphynes under shearing and bending, J. Appl. Phys. 119 (2016) 204304.
[16] J. Hou, Z.G. Yin, Y.Y. Zhang, T.C. Chang, An analytical molecular mechanics model for elastic properties of graphyne-n, J. Appl. Mech. 82 (2015) 094501.
[17] R. Couto, N. Silvestre, Finite element modelling and mechanical characterization of graphyne, J. Nanomater. 2016 (2016) 7487049.
[18] B. Liu, Y. Huang, H. Jiang, S. Qu, K.C. Hwang, The atomic-scale finite element method, Comput. Methods Appl. Mech. Eng. 193 (17) (2004) 1849–1864.
[19] B. Liu, H. Jiang, Y. Huang, S. Qu, M.F. Yu, K.C. Hwang, Atomic-scale finite element method in multiscale computation with applications to carbon nanotubes, Phys. Rev. B 72 (3) (2005) 035435.
[20] G.M. Odegard, T.S. Gates, L.M. Nicholson, K.E. Wise, Equivalent-continuum modeling of nano-structured materials, Compos. Sci. Technol. 62 (2002) 1869–1880.
[21] P.M. Morse, Diatomic molecules according to the wave mechanics. II. Vibrational levels, Phys. Rev. 34 (1929) 57–64.
[22] J. Lennard-Jones, On the determination of molecular fields: II: from the equation of state of a gas, Proc. R. Soc. Lond. Ser. A 106 (738) (1924) 463–477.
[23] T. Belytschko, S.P. Xiao, G.C. Schatz, R. Ruoff, Atomistic simulations of nanotube fracture, Phys. Rev. B 65 (2002) 235430.
[24] S.J. Blanksby, G.B. Ellison, Bond dissociation energies of organic molecules, Acc. Chem. Res. 4 (2003) 255–263.
[25] R. Rafiee, M. Heidarhaei, Investigation of chirality and diameter effects on the Young's modulus of carbon nanotubes using non-linear potentials, Compos. Struct. 94 (2012) 2460–2464.
[26] G.M. Odegard, T.S. Gates, K.E. Wise, C. Park, E.J. Siochi, Constitutive modeling of nanotube-reinforced polymer composites, Compos. Sci. Technol. 63 (2003) 1671–1687.
[27] S. Georgantzinos, D. Katsareas, N. Anifantis, Graphene characterization: a fully non-linear spring-based finite element prediction, Physica E 43 (2011) 1833–1839.
[28] F.P. Beer, Mechanics of Materials, McGraw-Hill Higher Education, New York, 2009.
[29] Y. Yang, X. Xu, Mechanical properties of graphyne and its family – a molecular dynamics investigation, Comput. Mater. Sci. 61 (2012) 83–88.
[30] S. Ajori, R. Ansari, M. Mirnezhad, Mechanical properties of defective gamma-graphyne using molecular dynamics simulations, Mater. Sci. Eng. 561 (2013) 279–289.
[31] S. Rouhi, T. Pour Reza, B. Ramzani, S. Mehran, Investigation of the vibration and buckling of graphynes: a molecular dynamics-based finite element model", Proc. Inst. Mech. Eng. Part C: J. Mech. Eng. Sci. 231 (6) (2017) 1162–1178.
[32] J. Zhao, N. Wei, Z. Fan, L. Liang, T. Rabczuk, The mechanical properties of three types of carbon allotropes, Nanotechnology 24 (9) (2013) 095702.
[33] M. Asadpour, S. Malakpour, M. Faghihnasiri, B. Taghipour, Mechanical properties of two-dimensional graphyne sheet, analogous system of BN sheet and graphyne-like BN sheet, Solid State Commun. 212 (2015) 46–52.
[34] J.W. Eischen, S. Torquato, Determining elastic behavior of composites by the boundary element method, J. Appl. Phys. 74 (1) (1993) 159–170.